Journal Pre-proof

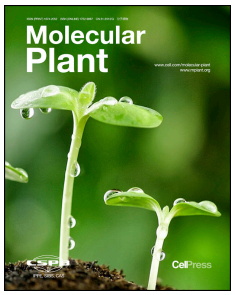

Manipulation of Photosensory and Circadian Signalling Restricts Phenotypic Plasticity in Response to Changing Environmental Conditions in Arabidopsis

Martin William Battle, Scott Fraser Ewing, Cathryn Dickson, Joseph Obaje, Kristen N. Edgeworth, Rebecca Bindbeutel, Rea Antoniou Kourounioti, Dmitri A. Nusinow, Matthew Alan Jones

PII: S1674-2052(24)00226-0

DOI: https://doi.org/10.1016/j.molp.2024.07.007

Reference: MOLP 1761

To appear in: *MOLECULAR PLANT*

Received Date: 15 March 2024

Revised Date: 14 June 2024

Accepted Date: 11 July 2024

Please cite this article as: Battle M.W., Ewing S.F., Dickson C., Obaje J., Edgeworth K.N., Bindbeutel R., Kourounioti R.A., Nusinow D.A., and Jones M.A. (2024). Manipulation of Photosensory and Circadian Signalling Restricts Phenotypic Plasticity in Response to Changing Environmental Conditions in Arabidopsis. Mol. Plant. doi: https://doi.org/10.1016/j.molp.2024.07.007.

Title Manipulation of Photosensory and Circadian Signalling Restricts Phenotypic Plasticity in Response to Changing Environmental Conditions in Arabidopsis

Author list
Martin William Battle[1]
Scott Fraser Ewing[1]
Cathryn Dickson[1]
Joseph Obaje[1,2]
Kristen N. Edgeworth[3,4]
Rebecca Bindbeutel[3]
Rea Antoniou Kourounioti[1]
Dmitri A. Nusinow[3,5]
Matthew Alan Jones[1,5]

1 Plant Science Group
School of Molecular Biosciences
University of Glasgow
Glasgow
G12 8QQ
United Kingdom

2 Current address: School of Biological and Environmental Sciences
Liverpool John Moores' University
Liverpool
L2 2QP
United Kingdom

3 Danforth Plant Science Center
St. Louis
Missouri
MO 63132
USA

4 Department of Biological and Biomedical Sciences
Washington University in St. Louis
St. Louis
MO 63130
USA

Contact: matt.jones@glasgow.ac.uk , meter@danforthcenter.org

Short summary: Plants utilise phenotypic plasticity to adapt to prevailing environmental conditions. Our data demonstrate that manipulation of phytochromeB- and EARLY FLOWERING3-regulated signalling pathways can limit phenotypic plasticity regardless of light and temperature signals. This has implications for future crop

development by promoting consistent plant growth and development despite the effects of climate change.

Abstract

Plants exploit phenotypic plasticity to adapt their growth and development to prevailing environmental conditions. Interpretation of light and temperature signals are aided by the circadian system which provides a temporal context. Phenotypic plasticity provides a selective and competitive advantage in nature but is obstructive during large-scale, intensive agricultural practices since economically important traits (including vegetative growth and flowering time) can widely vary depending on local environmental conditions. This prevents accurate prediction of harvesting times and produces a variable crop. We sought to restrict phenotypic plasticity and circadian regulation by manipulating signalling systems that govern plants' responses to environmental signals. Mathematical modelling of plant growth and development predicted reduced plant responses to changing environments when circadian and light signaling pathways were manipulated. We tested this hypothesis by utilising a constitutively-active allele of the plant photoreceptor phytochromeB, along with disruption of the circadian system via mutation of *EARLY FLOWERING3.* We found that these manipulations produced plants that were less responsive to light and temperature cues and which failed to anticipate dawn. These engineered plants have uniform vegetative growth and flowering time, demonstrating how phenotypic plasticity can be limited whilst maintaining plant productivity. This has significant implications for future agriculture in both open fields and controlled environments.

Keywords

Circadian, Developmental plasticity, Phenotypic plasticity, External coincidence, Light, Temperature

Introduction

Phenotypic plasticity enables plants to adapt to micro-niches within their environment but is problematic in modern agriculture which benefits from uniform and predictable growth and reliable harvest times. In addition to experiencing daily and seasonal climatic differences, plants respond to light and temperature signals differentially

dependent upon time of day (Millar, 2016). Photo- and thermo-sensors work in combination with the circadian system which provides an internal timing reference relative to dawn and dusk (Sanchez et al., 2020, Kerbler and Wigge, 2023). The plant circadian system continually integrates light and temperature as entrainment signals to modulate development, with a suite of photoreceptors including phytochromes (phyA through phyE), cryptochromes (cry1-3), zeitlupe (ZTL), and UVR8 each integrate light signals into the circadian clock (Somers et al., 2004, Fehér et al., 2011, Somers et al., 1998, Sanchez et al., 2020, Webb et al. 2019). Phytochromes have been proposed to associate with promoters to alter gene expression, in part by specifying alternate promoter selection although a role for phytochromes as transcriptional repressors has also been proposed (Jung et al., 2016, Ushijima et al., 2017, Chen et al., 2014, Balcerowicz et al., 2021). In line with this, phyB has been shown to interact with EARLY FLOWERING3 (ELF3), a chromatin-associated transcriptional repressor with a vital role in the circadian system (Liu et al., 2001, Covington et al., 2001, McWatters et al., 2000, Thines and Harmon, 2010, Huang et al., 2016a).

ELF3 was originally identified from a mutant screen to identify lines with accelerated flowering but was quickly noted to be essential for the maintenance of circadian rhythms in constant light (Hicks et al., 1996, Zagotta et al., 1996). Detailed studies suggest that the inhibition of circadian rhythms under constant illumination is caused by the loss of circadian gating of light signaling (McWatters et al., 2000, Thines and Harmon, 2010). Later work described ELF3 as an integral part of the Evening Complex that enables interactions between ELF4 and LUX ARRHYTHMO and which represses gene expression during the night (Nusinow et al., 2011). Higher-order mutant analyses and genome-wide studies demonstrate that phyB and ELF3 have additive roles in regulating hypocotyl length and flowering time (Reed et al., 2000, Ezer et al., 2017), while *phyb* exacerbates the shortened circadian free-running period of *elf3-12* seedlings (Kolmos et al., 2011). Interestingly, ELF3 and phyB have both been shown to be responsive to temperature as well as contributing to circadian timing and photoperception (Jung et al., 2016, Jung et al., 2020, Legris et al., 2016).

Although phyB and ELF3 bind one another, we still do not understand how ELF3 and phyB interact to maintain circadian rhythms and regulate plant development (Huang et al., 2016a, Liu et al., 2001). Here, we have revised mathematical models of the circadian system to better interpret phyB and ELF3 interactions, and have utilised a constitutively active allele of phyB (Y276®H, YHB) in combination with a null *ELF3* allele to examine whether these crucial components of plants' sensory system can be engineered to limit plants responses to environmental cues.

Results and Discussion

Modelling refines our understanding of light input into the circadian system

Decades of research suggest that phyB- and ELF3-signalling pathways are genetically separable, although multiple lines of evidence demonstrate a functional interaction between these signalling pathways (Reed et al., 2000, Kolmos et al., 2011, Covington et al., 2001, Jung et al., 2016, Legris et al., 2016, Liu et al., 2001, Yu et al., 2008, Nieto et al., 2022). Mathematical modelling of these interactions highlights the central contributions of phyB and ELF3 towards key aspects of development such as seedling establishment and flowering time (Chew et al., 2022, Seaton et al., 2015). Disruption of ELF3 function induces consistently early flowering, yet imposes an etiolated phenotype that is reproduced by the Arabidopsis Framework Model [FMv2; Fig. S1A-C, (Chew et al., 2022, Seaton et al., 2015)]. Since increased phyB activity (either through over-expression or inclusion of a constitutively-active YHB allele) promotes photomorphogenesis via post-translational regulation of PIFs, we expected that YHB would be epistatic to *elf3* with regards photomorphogenesis (Hajdu et al., 2015, Su and Lagarias, 2007, Wagner et al., 1991). FMv2 aligned with our hypothesis that increased phyB signalling in the absence of ELF3 (modelled by increasing light inputs into the P2012 circadian module and S2015 photoperiodism module) would limit hypocotyl growth whilst retaining an early flowering phenotype (Fig. S1A-C).

Plants expressing *YHB* maintain robust circadian rhythms in constant darkness compared to wild type, although it remains unclear how phyB-initiated signals are integrated into the

circadian system (Jones et al., 2015, Huang et al., 2019). We examined two alternate hypotheses to apply constitutive phyB signalling into the circadian module of FMv2 (Fig. S1D). Initially we investigated whether constitutive phyB signalling acted by promoting light-induced gene expression within the model, as well as repressing COP1 accumulation (Fig. S1D). This 'global phyB effect' could not reconstitute YHB-mediated circadian rhythms in FMv2 after transfer to constant darkness (Fig. S1E). Interestingly, work examining dawn-induced gene expression suggests that photoreceptor activation is insufficient to promote transcript accumulation (Balcerowicz et al., 2021). Removing light-activated gene expression from our YHB simulation provided a 'COP1 only' variant (Fig. S1D, S1F). The FMv2+COP1 variant retained circadian rhythms in constant darkness but was inconsistent with previous experimental data since circadian behaviour was similar to wild type and the early flowering phenotype of *YHB* plants was not predicted [Fig. S1D, S1F; (Pokhilko et al., 2012, Fogelmark and Troein, 2014, Jones et al., 2015, Hajdu et al. 2015, Huang et al., 2019)].

This inconsistency within the model when compared to experimental data encouraged us to examine alternate circadian models. The F2014 circadian model revises the FMv2 circadian module to include refined waves of transcriptional repression based on experimental data (Fogelmark and Troein, 2014). The resultant 'FMv2+F2014' model recapitulated YHB-mediated retention of circadian amplitude compared to damping in wild type, although the model was unable to recapitulate the extension of circadian period observed in YHB lines in constant darkness (Fig. 1; Huang et al. 2019; Jones et al. 2015). The effect of YHB was apparent in both 'global' and 'COP1 only' approximations of YHB, although again the 'COP1 only' variant matched the experimental luciferase data more closely [Figs. 1B-D; (Huang et al., 2019, Jones et al., 2015)]. Future model iterations incorporating transcriptional regulation from photosynthetically-derived signals could further improve model predictions, particularly with regards phase and period length (Queiroz et al., 2023). We next examined how disruption of *ELF3* was predicted to affect constitutive phyB signalling. Both FMv2 and FMv2+F2014 models predict *elf3* will be epistatic to *YHB* regarding circadian rhythmicity [Fig. 1 and S1; (Thines and Harmon, 2010, McWatters et al., 2000, Covington et al., 2001, Huang et al., 2016a)].

The combination of *YHB* and *elf3* alleles restricts daily patterns of gene expression

We next sought to reproduce these predictions *in planta* by introducing the *YHB* allele into *elf3* (Hu et al., 2009, Su and Lagarias, 2007, Nusinow et al. 2011). This allowed us to assess whether *YHBelf3* seedlings had phenotypes aligned with our modelled predictions, with the ultimate goal of minimising phenotypic plasticity and circadian regulation in plants (Fig. 2). *In vivo,* neither constitutive expression of *YHB* [*35S::YHB* (*elf3-1 phyb-9*)] nor expression of *YHB* driven by the endogenous *PHYB* promoter [*PHYB::YHB* (*elf3-2); YHBelf3-2*] were able to maintain circadian rhythms of *CCA1*-driven bioluminescence in constant darkness, with only 15% of *YHBelf3-2* lines being assessed as rhythmic [Fig. 2A-B and Fig. S2A-B; (Jones et al., 2015, Huang et al., 2019)]. qRT-PCR analysis of candidate genes (including *CCA1, LHY, GIGANTEA,* and *PSEUDORESPONSE REGULATOR9; PRR9*) confirmed the loss of circadian rhythmicity in *YHBelf3-2* lines compared to *YHB* (Fig. 1C). Interestingly, mis-regulation of these candidate circadian transcripts fell into two groups; *CCA1*/*LHY* [whose promoters are solely bound by phyB; Fig. S3; (Ezer et al., 2017, Jung et al., 2016)] and *GI/PRR9* [bound by both phyB and ELF3; Fig. S3; (Ezer et al., 2017, Jung et al., 2016)]. For each transcript, accumulation patterns over time were consistent in *elf3-2* and *YHBelf3-2* seedlings (Fig. 1C). Although the FMv2+F2014 model aligned with experimental transcript accumulation for *CCA1, LHY*, and *GIGANTEA*, we were interested to note that the FMv2+F2014 model predicted *PRR9* mRNA to damp to basal levels in *elf3* and *YHBelf3* plants (Fig. 1D). This contrasts our experimental data which demonstrates elevated (and arhythmic) *PRR9* accumulation in *elf3*-2 and *YHBelf3-2* plants (Fig. 1D). Such data indicate that ELF3 is necessary to retain circadian rhythms yet highlights the limitations of existing mathematical models to fully reconstitute the circadian system.

ELF3 and YHB signallling programmes interact to affect photomorphogenic and circadian gene expression programs

To further explore the regulation of gene expression in *YHBelf3-2* seedlings we used RNA sequencing to assess transcript accumulation in plants 48hrs after transfer to constant darkness at dusk (ZT60), a time point at which wild-type seedlings appeared to have

become arrhythmic and therefore had relatively stable levels of circadian-controlled transcript abundance (Figs. 1C, 2A, S4). Although starvation markers were upregulated in all genotypes (e.g. ATL8 and KMD4; Graf et al. 2010), circadian rhythms persisted in *YHB* seedlings at ZT60, suggesting that circadian rhythms are actively damped in a phyB-dependent manner (Jones et al. 2015, Huang et al. 2019).

We first determined log fold change (-log2FC) in each of *elf3-2*, *YHB,* and *YHBelf3-2* genotypes relative to wild type (Fig. S4, Table S1). As expected, GO terms associated with responses to light stimuli were over-represented in our lists of genes mis-expressed in *YHB* and *YHBelf3-2* (Fig. S5, Table S2). GO terms associated with circadian rhythms were also significantly over-represented (Fig. S5, Table S2). We next examined whether mis-regulated transcripts in each genotype tended to be expressed at particular times of day by assessing whether mis-expressed genes were over- or under-represented at particular times of day [Fig. 2C; (Bonnot et al., 2022)]. Significantly mis-accumulated transcripts were not confined to a single time period in *elf3-2*, *YHB,* or *YHBelf3-2* lines, suggesting that the circadian system is not 'locked' at a particular circadian phase in any of these genotypes (Fig. 2C). Instead, differences in the accumulation of numerous core circadian transcripts were apparent [Fig. S4A-D; (Hsu and Harmer, 2014, Laosuntisuk et al., 2023)]. In constant darkness, *elf3-2* plants accumulate increased levels of *GIGANTEA, PRR9,* and *BROTHER OF LUX ARRHYTHMO* whereas *CCA1, LHY,* and *REVEILLE8* (*RVE8*) steady-state levels are reduced (Fig. S4A). 10 of the notional 60 core clock genes are highly mis-accumulated in *YHB* relative to wild type (9 upregulated and 1 downregulated; Fig. S4A, S4C).

To further address how YHB and ELF3 govern photomorphogenesis, we examined differential expression of genes associated with a response to light stimuli using our RNAseq dataset of dark-adapted plants (Fig. S4E-H; [GO:0009416; (Ashburner et al., 2000, Gene Ontology Consortium, 2023)]). Of the 740 light stimulus-associated transcripts examined, only 33 are mis-regulated in *elf3-2* plants, with six downregulated and 27 upregulated transcripts (Table S1). Of these, *elf3-2* and *YHBelf3-2* plants share only 7 mis-regulated transcripts, one of which (*HOMEOBOX-LEUCINE ZIPPER*

PROTEIN 4; HB4) has previously been shown to play a role in shade avoidance via both phytochrome signalling and ELF3 [Fig. S4E-H, (Sorin et al., 2009, Jiang et al., 2019)]. *HB4* is downregulated in *elf3-2* but upregulated in *YHB* and *YHBelf3-2* (Fig. S4E-H, Table S1). By contrast, 113 transcripts are significantly differentially expressed in *YHB* plants relative to wild type, with 83 being upregulated and 30 downregulated (Figs. S4G-H, Table S1). 91 of these transcripts are similarly differentially expressed in both *YHB* and *YHBelf3-2* plants (Fig. S4G-H).

We further dissected interactions between *YHB*- and *elf3*-affected transcript accumulation by assessing differential gene expression in *YHBelf3-2* seedlings compared to either *YHB* or *elf3-2* (Figure S4I-M). There was little correlation in expression levels between genes differentially expressed in *elf3-2* relative to Col-0 and *YHBelf3-2* relative to *YHB*, suggesting that the loss of ELF3 has different effects upon global transcript accumulation in the presence or absence of YHB (Figure S4I, $R < 0.35$). However, we observed a strong correlation in differential gene expression when comparing transcripts mis-expressed in *YHB* relative to Col-0 and *YHBelf3-2* relative to *elf3-2* (Figure S4J, $R > 0.8$). This correlation was retained both when we divided our data into circadian-regulated and circadian-independent transcripts, and also when we assessed the accumulation of light responsive transcripts (Figure S4J, S4L). These data suggest an epistatic effect of constitutive phyB signalling upon photomorphogenesis despite the inter-related nature of phyB- and ELF3-mediated effects upon gene expression (Nieto et al., 2022).

By comparison, ELF3 had a stronger role in regulating core circadian transcripts (Figure S4M-S4N). *YHB* expression continued to affect the accumulation of some core circadian transcripts in the absence of ELF3 but the majority of differentially expressed core clock transcripts were well correlated (when comparing *elf3-2* relative to Col-0 and *YHBelf3-2* relative to *YHB*; Figure S4M, R = 0.8). Equally, the mis-expression of numerous core circadian transcripts was altered when comparing *YHB* relative to Col-0 and *YHBelf3-2* relative to *elf3-2* (Figure S4N). These data align with the essential role of *ELF3* within the circadian system (Covington et al. 2001; Thines et al. 2010) whilst highlighting putative loci where YHB affects core clock transcript accumulation separately from ELF3.

265

266 ***YHBelf3* plants have a reduced response to light:dark cycles compared to wild type**

267 We next examined the behaviour of *YHBelf3* seedlings in the presence of light. Although
268 our modelling expected that *elf3* and *YHBelf3* would essentially be arhythmic in response
269 to dawn and dusk (Fig. 2D), each of the genotypes examined displayed circadian
270 entrainment to experimental light signals and retained daily responses to dawn, as
271 depicted by the calculated phase of *CCA1::LUC2* bioluminescence in driven light:dark
272 cycles (Fig. 2E-F). *CCA1::LUC2* bioluminescence began to increase in wild-type and *YHB*
273 seedlings 1-3 hours before dawn, indicating a circadian anticipation of dawn in these
274 plants (Fig. 2E). By contrast, this dawn anticipation was absent in *elf3-2* and *YHBelf3-2*
275 plants, with *CCA1::LUC2* driven bioluminescence increasing only after the application of
276 light (Fig. 2E). These data suggest that *elf3-2* and *YHBelf3-2* retain photosensitivity
277 despite the disruption of circadian rhythmicity in these lines.

278

279 Since *elf3-2* and *YHBelf3-2* plants retained a response to dawn, we examined the
280 activation of the *CCA1* promoter in response to varied light intensity during the
281 photoperiod (Fig. 2G-H). A pseudo-sinusoidal regime was designed, where light intensity
282 varied throughout the day, peaking in the late morning and gradually decreasing as dusk
283 approached (Fig. 2G). Our experimental data demonstrated that *elf3-2* retained
284 entrainment to pseudo-sinusoidal lighting, although *YHBelf3-2* was less able to entrain to
285 these conditions (Fig. 2G-H). These data are consistent with additional photosensory
286 systems feeding into the regulation of *CCA1*, including metabolic signals from
287 photosynthesis (Jones, 2018, Jones, 2019, Wang et al., 2024, Haydon et al., 2013).

288

289 We next assessed circadian rhythmicity in *YHBelf3* seedlings held in constant light. Our
290 modelling predicted that wild-type and *YHB* seedlings would have comparable circadian
291 rhythms in constant light (Fig. 2I). In line with this hypothesis, circadian rhythms in *YHB*
292 seedlings were indistinguishable from wild type in constant white light, although the phase
293 of *CCA1::LUC+* activity was approximately 6 hours later than modelled *CCA1* mRNA (Fig.
294 2I-K). This delay in phase may reflect time required for luciferase translation or could
295 indicate that light inputs into the F2014 model require further refinement to include

296 photosynthetic signals or additional photoreceptor control. Despite these caveats, the
297 model was able to reproduce the dissipation of circadian rhythms in *elf3-2* and *YHBelf3-*
298 *2* seedlings within 24 hours of transfer to constant white light (Fig. 2J-K).
299
300 **_YHBelf3-2_ plants have reduced growth and flowering plasticity in response to light**
301 **and temperature cues**
302 The combination of *YHB* and *elf3* alleles decouples the circadian system from
303 photomorphogenesis, although *YHBelf3-2* plants can retain daily patterns of gene
304 expression when grown in light:dark cycles (Figs. 1 + 2). We were therefore interested
305 how our genetic manipulations affected developmental traits and life cycle transitions in
306 varied light conditions (Fig. 3). Our FMv2+F2014 model predicted that hypocotyl length
307 would be uncoupled from photoperiod in *YHBelf3* (Fig. 3A). We observed that *YHB*-driven
308 growth phenotypes persisted in the hypocotyls of 5-day old seedlings (Fig. 3B-D).
309 *YHBelf3-2* seedlings retained a short hypocotyl phenotype regardless of the light
310 condition utilised for growth and with no significant difference observed between *YHB* and
311 *YHBelf3-2* seedlings (Fig. 3B-D). We note that *YHB* and *YHBelf3-2* seedlings were
312 indistinguishable from wild type when grown under long-day conditions (Fig. 3D). Ranking
313 of phenotypic plasticity between genotypes highlighted that hypocotyl length of *elf3-2*
314 seedlings was more sensitive to photoperiod than wild type whereas *YHB* and *YHBelf3-*
315 *2* seedlings were less responsive [Table S4; (Arnold et al. 2019)].
316
317 We next examined growth phenotypes in more mature Arabidopsis plants (3 weeks after
318 sowing; Fig. 3E-F, S6). The size of wild-type Arabidopsis plants is greatly dependent upon
319 photoperiod length when plants are grown at 22°C, with rosette diameter decreasing as
320 photoperiod increases (Fig. 3E-F). *elf3-2* seedlings had an expanded rosette diameter
321 compared to wild-type grown under long days, possibly related to the loss of light
322 perception in these lines [Fig. 3E-F; (Zagotta et al., 1996)]. We noted substantial variation
323 in rosette diameter in wild-type and *elf3-2* plants, although rosette diameter was more
324 consistent under longer photoperiods (Fig. 3E-F). By contrast, the rosette of *YHB* and
325 *YHBelf3-2* seedlings were indistinguishable from each other, being more compact and
326 uniform in size regardless of daylength (Fig. 3E-F).

YHB and *elf3-2* genotypes have both previously been shown to have an early flowering phenotype when grown under short-day conditions and so we expected that *YHBelf3-2* plants would share this phenotype [Fig. 3G-H; (Franklin and Quail, 2010, Hajdu et al., 2015, Zagotta et al., 1996)]. Our FMv2+F2014 model similarly predicts that *YHBelf3* plants will display reduced photoperiodic sensitivity comparable to *elf3* (Fig. 3G). In agreement with this hypothesis, *YHB*, *elf3*, and *YHBelf3-2* plants flowered earlier than wild type under either long-day or short-day conditions (Fig. 3G-H).

Both phyB and ELF3 are critical for temperature responses in addition to their roles in photoperception (Jung et al., 2020, Jung et al., 2016, Legris et al., 2016). We therefore compared how our *YHBelf3-2* plants performed under varying temperature conditions (Fig. 4). In contrast to light-driven entrainment (Figs. 2E-F), *CCA1*-driven bioluminescence peaked 6 hours after dawn in wild-type when entrained to temperature (Fig. 4A-B). The phase of *CCA1*-driven bioluminescence was unaffected in *YHB* seedlings, although neither *elf3-2* nor *YHBelf3-2* seedlings could entrain to temperature signals when held in constant light (Fig. 4A-B). These data suggest that light cues are necessary to drive rhythmic *CCA1* expression in *elf3* and *YHBelf3-2* seedlings.

As under different lighting regimes, *elf3-2* hypocotyls displayed greater plasticity than wild type, with *YHB* and *YHBelf3-2* hypocotyls being less responsive to temperature than wild type [Fig. 4C, Table S4; (Arnold et al. 2019)]. Seedling growth is therefore more uniform in *YHBelf3-2* plants compared to wild type regardless of light or temperature cues, as previously reported for *YHB* alone (Jung et al. 2016). Ambient temperature also affected rosette diameter (Figs. 4D, S6). Wild-type plants maintain a comparatively consistent diameter between 12°C and 27°C when grown in neutral day conditions (12:12 light:dark cycles), with a modest yet significant decrease at 12°C (Fig. 4D, Fig. S6, Table S4). By contrast, *elf3-2* seedlings were more sensitive to lower temperatures, with rosette diameter substantially decreasing at 12°C and 17°C compared to higher temperatures (Fig. 4D, Table S4). *YHB* and *YHBelf3-2* plants were also responsive to these temperature changes although the difference in size was smaller than observed in *elf3-2*

plants (Fig. 4D, Table S4). Under neutral day conditions, flowering was delayed in all genotypes when plants were grown at 12°C, but we were interested to note that *YHBelf3-2* plants flowered earlier than *YHB* in contrast to other developmental phenotypes where *YHB* effects were epistatic (Fig. 4E, Table S4). Flowering time accelerated in wild-type plants as temperatures increased (Fig. 4E, Table S4). By contrast, *YHB*, *elf3-2,* and *YHBelf3-2* genotypes retained stable flowering times from 17°C to 27°C (Fig. 4E). The *YHB* and *YHBelf3-2* plants therefore retain uniform and early flowering phenotypes and so demonstrate reduced phenotypic plasticity across a range of light conditions and temperatures.

Photo- and thermo-morphogenesis are crucial processes that enable plants to optimise growth and development in response to prevailing environmental conditions by phenotypic plasticity. Our data validate mathematical models and demonstrate that expression of *YHB* is epistatic to the morphological consequences of *ELF3* disruption, although *ELF3* is essential to maintain circadian rhythmicity (Fig.1-3). *YHBelf3-2* plants consequently retain a vegetative phenotype comparable to wild-type yet have an early flowering phenotype and cannot anticipate daily environmental transitions (Figs. 3-4). The combination of *YHB* and *elf3* alleles consequently produces plants less responsive to environmental signals that retain vegetative growth and predictable flowering. This demonstrates how engineering the circadian system alongside environmental signalling pathways creates plants with more uniform growth and consistent environmental responses.

Although phenotypic plasticity is advantageous in natural conditions (where competition for resources and environmental stresses vary across seasons and locations) this trait is disadvantageous in modern crop monoculture where fertilisers, pesticides, irrigation, etc., can be provided. Reducing phenotypic plasticity and circadian regulation has potential beneficial implications for farming, and one goal of modern breeding programmes has been to increase the uniformity of crops so that harvesting time is more predictable and quality is consistent. This applies to intensive, precision outdoor farming and Total Controlled Environment Agriculture (TCEA, or vertical farming). In addition, climate

change has rapidly altered daylength and temperature relationships worldwide, and maintaining crop productivity in current locations or moving to more favourable temperate latitudes will require manipulation of environmental responses. Our modelling predicted that manipulating phyB and ELF3 signalling cascades would restrict phenotypic plasticity and circadian regulation in response to changing photoperiods (Figs. 1-3). Crucially, we have shown that combining these two alleles [*YHBelf3*] limits phenotypic plasticity and circadian regulation while retaining earlier flowering times and maintaining vegetative growth (Fig. 3-4). Since ELF3 and YHB have conserved function across species it will be of great interest to apply these genetic modifications to reduce developmental variation in crops (Huang et al., 2017, Hu et al., 2020).

Methods

Plant Material and Growth Conditions

Wild type *CCA1::LUC*+, and *elf3-2 CCA1::LUC*+ Arabidopsis seed have previously been reported (Huang et al., 2016a). *PHYB::YHB* and *PHYB::YHB* (*elf3-2*) Arabidopsis were generated by transforming *CCA1::LUC*+, and *elf3-2 CCA1::LUC*+ seed with pJM63 gYHB (Su and Lagarias, 2007) via floral dip (Clough and Bent, 1998). Transformants were selected with 75mg mL^{-1} kanamycin to identify homozygous seedlings in the T3 generation. *phyb-9 elf3-1* lines were generated by crossing *elf3-1* to CCA1::LUC+ and *phyB-9* was crossed to CCA1::LUC+, with long hypocotyl, bioluminescent F2 seedlings confirmed for homozygous *elf3-1* and *phyB-9* alleles using a dCAPS primer strategy as described previously (Nusinow et al., 2011, Huang et al., 2016b). *elf3-1* CCA1::LUC+ was then crossed to *elf3-1 phyB-9* (Reed et al., 2000), and bioluminescent, long hypocotyl F2 lines were confirmed as *elf3-1 phyB-9* using dCAPS primers. F3 lines were screened for bioluminescence to identify homozygous CCA1::LUC+ seedlings.

CER was cloned from plasmid CER C1 (Koushik et al., 2006) using primers pDAN0869 and pDAN0870 and recombined with pB7-SHHc (Huang et al., 2016b) digested with AvrII using In-Fusion HD cloning (Clontech, Mountain View, CA) to generate pB7-CER-SHHc. pENTR-YHB (Huang et al., 2016b) was recombined with pB7-CER-SHHc to generate pB7-YHB-CER-SHHc. This plasmid was transformed into *elf3-1 phyb-9*

CCA1::LUC+ to generate *35S::PHYB(elf3-1 phyb*-9) *CCA1::LUC*+ and transformants were identified by BASTA resistance.

T3 and F3 seed were surface sterilised in chlorine gas and stratified in sterile water at 4°C for at least three days prior to plating on half-strength Murashige and Skoog (0.5 MS) medium (Prasetyaningrum et al., 2023). Seedlings were entrained for 5–12 d before being transferred to testing conditions as described in each figure legend. During standard growth, plants were kept under 150 µmol m^{-2} s^{-1} white light in 12 hrs:12 hrs light:dark cycles in Panasonic MLR-352-PE chambers. Relative humidity and temperature were set to 60–70% and 22°C, respectively except where growth under other temperatures conditions are listed.

Hypocotyl assays

Seeds were grown on 0.5 MS agar plates and irradiated with cool fluorescent white light at 170 µmol m^{-2} s^{-1} for 4 hr before being moved to LED chambers as per experimental requirements and grown vertically for 5 days before being imaged and processed using ImageJ (Schneider et al., 2012). Short day, long day and squareform treatments used 30 µmol m^{-2} s^{-1} and the pseudo-sinusoidal light treatment used a cycle of 1hr 10 µmol m^{-2} s^{-1}, 8hrs 40 µmol m^{-2} s^{-1}, 5hrs 30 µmol m^{-2} s^{-1}, 4hrs 10 µmol m^{-2} s^{-1} and 6hrs darkness. Data were plotted and analysed using a One-way ANOVA followed by Dunnett's multiple comparisons test in GraphPad Prism version 10.0.3.

Luciferase assays

Individual seedlings were grown for 6 days in 12:12 light:dark cycles under white light on half-strength MS media as in previous work (Prasetyaningrum et al., 2023). Plants were sprayed with 3 mM D-luciferin in 0.1% Triton X-100, before being transferred to imaging conditions as described for each experiment. Individual plants were imaged repeatedly (every 1-2 hours) dependent upon the experiment using a Retiga LUMO camera run by MicroManager 1.4.23 (Edelstein et al., 2014) using a custom script. In experiments where temperature was not constant throughout growth and imaging, temperature change was initiated as indicated. The patterns of the luciferase signal

were fitted to cosine waves using Fourier Fast Transform-Non-Linear Least Squares [FFT-NLLS; (Plautz et al., 1997)] to estimate the circadian period length made using BioDare2 [(Zielinski et al., 2014); biodare2.ed.ac.uk]. Relative Amplitude Error (RAE) was calculated by dividing the amplitude error estimate for each curve by the amplitude value (Plautz et al., 1997). Data were considered rhythmic if the fitted curve returned a period estimate within 18-34hrs and had an RAE<0.6. Waveforms, periods and percentage rhythmicity data were plotted using GraphPad Prism version 10.0.3.

qRT-PCR

Following entrainment, seedlings were transferred to constant darkness at dusk. Tissue was harvested and snap-frozen in liquid nitrogen at the indicated time points before RNA extraction using using Tri Reagent® according to the manufacturer's protocol (Sigma Aldrich, Dorset, UK, http://www.sigmaaldrich.com). Reverse transcription was performed using either Superscript™ II or M-MLV reverse transcriptase according to manufacturer's protocols (Invitrogen, Waltham, Massachusetts, USA, https://www.thermofisher.com/Invitrogen). Real-time reverse transcription polymerase chain reaction was performed using a QuantStudio™ 3 Real-Time PCR System or a StepOnePlus™ Real-Time PCR System (Applied Biosystems, Waltham, Massachusetts, USA, https://www.thermofisher.com/AppliedBiosystems). Samples were run in triplicate and starting quantities were estimated from a critical threshold using the standard curve of amplification. *APA1*, *APX3* and *IPP2* expression was used as an internal control, with data for each sample normalised to these as previously described (Nusinow et al., 2011).

RNAseq

Plants were grown on 0.5 MS agar plates under entrainment conditions for 12 days. At dusk on the twelfth day of growth (ZT12), seedlings were transferred to constant darkness. Pools of ca. 20 seedlings were harvested and snap-frozen in liquid nitrogen 48 hours later (ZT60). Total RNA was extracted from three biological replicates per genotype using Tri Reagent® according to the manufacturer's protocol (Sigma Aldrich, Dorset, UK, http://www.sigmaaldrich.com). Library preparation and Illumina sequencing

(Illumina, San Diego, USA) with 150bp paired-end reads was performed by Novogene Biotech (Cambridge, UK) using Illumina protocols. RNAseq reads were first aligned to the AtRTD3 transcriptome (Zhang et al., 2022) and read-counts were generated using Kallisto (Bray et al., 2016) in the Galaxy platform (Afgan et al., 2016). Subsequent analysis was performed using the 3DRNAseq pipeline (Guo et al., 2021). Transcript abundance was expressed as Transcripts Per Million (TPM) for each gene product within each genotype. TPM values were used to calculate fold change difference in transcript accumulation relative to other genotypes. Analysis of variance (ANOVA) was performed to compare the transcript abundance (TPM) for a given transcript in each genotype to the other genotypes tested. This was followed by pairwise comparison via a post-hoc Tukey test to determine the adjusted *p*-values for each genotype pairing. Significant differential expression of a transcript was defined as two genotypes presenting a fold change difference of accumulation of -log2FC > 1 or -log2FC < -1 along with an adjusted *p*-value < 0.05. A list of transcripts contributing to circadian rhythmicity were derived from (Hsu and Harmer, 2014, Laosuntisuk et al., 2023). Gene ontology annotation was performed using DAVID (Huang et al., 2009, Sherman et al., 2022). A list of 740 genes were taken from the GO term GO:0009416 response to light stimulus (Ashburner et al., 2000, Gene Ontology Consortium, 2023). Genes of interest were plotted in heatmaps and volcano plots using R (R Core Team, 2013) and RStudio (Posit Software).

Phase enrichment analysis was completed using CAST-R (Bonnot et al. 2022). Differentially-accumulated transcripts for each genotype (Table S1) were compared to the “Bonnot and Nagel Transcriptome LL” reference dataset. Data was summarised by presenting fold enrichment (i.e. the ratio between the proportion of the phase in the genotype-specific mis-regulated gene list and the proportion in the defined phase reference dataset (Bonnot et al. 2022). Statistical significance was determined using a Chi-square test (Bonnot et al. 2022). Data were plotted using R (R Core Team, 2013) and RStudio (Posit Software).

Flowering time and growth analysis

Following stratification, plants were grown on soil until bolting. Rosette area, rosette diameter and leaf counts were measured regularly throughout the growth period (ca. twice per week). The number of days to bolting were recorded when the bolt was 1cm above the rosette. Plants were grown under 150 µmol m^{-2} s^{-1} white light with day length and temperature varied between experiments. For variable day length experiments, plants were grown under long-days (16 hrs light: 8 hrs darkness) or short-days (8 hrs light: 16 hrs darkness) at 22°C. For temperature response experiments, plants were grown under balanced day lengths (12 hrs light: 12h hrs dark) under either 27°C, 22°C, 17°C or 12°C. Data were plotted and analysed using a two-way ANOVA followed by Tukey's multiple comparisons test in GraphPad Prism version 10.0.3.

Ranking of phenotypic plasticity

Random regression mixed models were utilised to enable comparison of phenotypic plasticity between genotypes (Arnold et al. 2019). Akaike Information Criterion (AIC) were used to evaluate model fit (Zuur et al. 2009). Optimal model fits for hypocotyl length and flowering time were achieved by fitting a quadratic fixed effects model for the fixed effect of growth temperature or photoperiod, with random effects allocated to genotype. Rosette diameter was best modelled by fitting a cubic fixed effects model for the fixed effect of growth temperature, with random effects allocated to genotype.

Mathematical modelling

The Arabidopsis Framework Model version 2 (FMv2; Chew et al., 2022) is a multiscale model of Arabidopsis that brings together multiple modules to describe diverse processes including the circadian clock, flowering, metabolism and vegetative growth. The F2014 model (Fogelmark and Troein, 2014) is an updated Arabidopsis circadian clock model with fewer explicit light-sensitive reactions and without extended transcriptional activation. Both these models were used and combined in this study. The original FMv2 model was simulated, with minimal changes as described below to allow for introduction of the YHB mutant and for model comparison. The "FMv2+F2014" model was constructed by replacing the P2011 (Pokhilko et al., 2012) circadian module

of FMv2 with the updated F2014 circadian model, in the spirit of the modular Framework model.

FMv2 model: The MATLAB code for the FMv2 was downloaded from the github repository: https://github.com/danielseaton/frameworkmodel/ (FAIRDOM link: https://fairdomhub.org/models/248) and run in MATLAB R2022a.

Addition of F2014: MATLAB code was written to simulate the F2014 model based on the equations described in (Fogelmark and Troein, 2014). ChatGPT4 was initially used to convert the PDF image of the equations into LaTeX code. This was then manually corrected to remove errors introduced by the AI and then converted from LaTeX into MATLAB manually. Conversion to MATLAB was also performed using ChatGPT4, and the two were compared as an additional check.

The F2014 model replaced the P2011 module of the FMv2 model. Scaling factors were added to rescale the amplitudes of the outputs of the circadian module F2014 to match those of P2011, to allow input to the PIF-CO-FT (Seaton-Smith) module (Seaton et al., 2015). Furthermore, CCA1 and LHY are modelled separately in F2014, so the sum of the two was used to replace the LHY input to the PIF-CO-FT module. Specifically:

$$LHY_{P2011} = \frac{LHY_{F2014} + CCA1_{F2014}}{1.561}$$

$$PRR7_{P2011} = \frac{PRR7_{F2014}}{2.6754}$$

$$GIn_{P2011} = 40.9 \cdot GIn_{F2014}$$

$$PRR5_{P2011} = 0.841 \cdot PRR5n_{F2014}$$

$$TOC1_{P2011} = 1.21 \cdot TOC1n_{F2014}$$

Parameter choice: The parameter set 1 of (Fogelmark and Troein, 2014) was used in all simulations of this model. Parameters as preset in FMv2 were used for all other modules with the exception of parameters for the hypocotyl length calculation and the photothermal time threshold for flowering. These parameters were used unchanged for the mutant predictions.

Photothermal time threshold parameter for flowering: A single parameter value was used for both the FMv2 and the FMv2+F2014 models, which was fitted based on FMv2 using the laboratory's wildtype data for various photoperiods (Fig. S1B bottom panel). The parameter value was 4107.6 MPTU.

Hypocotyl length parameters: Hypocotyl length was calculated according to the equation used in (Seaton et al., 2015) :

$$Hyp_{length} = h_1 \int_0^{24} (z(t) - h_2)dt$$

where

$$z(t) = \begin{cases} c_{ATHB2}^{(m)}, & if\ c_{ATHB2}^{(m)} < h_3 \\ h_3, & if\ c_{ATHB2}^{(m)} \geq h_3 \end{cases}$$

Reparameterisation was carried out for h_1, h_2, h_3 separately for each version of the model based on the data shown in (Fig. S1B top panel).

Parameter	FMv2	FMv2 + F2014
h_1	0.2657	0.3747
h_2	-0.3595	-0.1844
h_3	0.6158	0.7107

Simulating Mutants: The *elf3* and YHB mutations were introduced in both P2011 and F2014 models. The *elf3* mutation is present in the original code for FMv2 (P2011), so this was simulated in the same way. For F2014, the ELF3 protein production parameter p_{16} was set to 0 in the mutant.

The YHB mutant was added in both circadian models, either "Globally" by altering all light inputs except for blue light (assumed to affect the GI and ZTL protein light-sensitivities and the dark accumulator) or by altering only COP1-related light inputs. The alteration in both cases was to set the relevant light input to be 75% ON in the dark (and 100% ON in the light as normal). This accounts for the activity of the constitutively active phyB signalling in the dark, and phyB in combination with wildtype signalling from other photoreceptors and photosynthetically-derived metabolites in the light. However,

we note that this value of 75% is not interpreted as the biological contribution of YHB to clock signalling but is chosen to account for observed changes in flowering time while still producing robust circadian rhythms (Fig. S7).

YHB is also affecting the PIF-CO-FT module directly, where phyB is explicitly modelled. In this case, the light variable only for the phyB equation itself is set to 1 at all times in the mutant.

Model simulation: The ODEs were solved numerically using MATLAB's ode15s. The circadian module for both P2011 and F2014 was initialised and entrained for 12 days in 12L/12D conditions prior to the simulation start. Initial conditions were set as in (Chew et al., 2022) for P2011, while for F2014 the initial value 0.1 was used for all variables.

Data Availability

Further information and requests for resources and reagents should be directed to and will be fulfilled by Matt Jones (matt.jones@glasgow.ac.uk). Plasmids generated in this study are available upon request. RNA-seq data have been deposited at GEO and are publicly available; PRJNA1078346. Luciferase data has been deposited in BioDare2 (www.biodare2.ac.uk) with accession numbers 29131 (Fig. 2A), 29135 (Fig. 2E), 29136 (Fig. 2G), 29133 (Fig. 2J), 29132 (Fig. 4A). Any additional information required to re-analyze the data reported in this paper is available from the corresponding authors upon request. Models of hypocotyl growth (Seaton et al., 2015) and flowering time (Chew et al., 2022) are derived from previously published work available at FAIRDOMHub: https://fairdomhub.org/models/248. All original code is publicly available at https://github.com/ReaAntKour/FMv2_F2014_model/releases/tag/v1.0.0.

Author contributions

Conceptualization, DAN, MAJ; Methodology, MWB, RAK, DAN, MAJ; Software, RAK; Validation, CD, JO, MWB; Formal Analysis, MWB, SFE, MAJ, JO; Investigation, MWB, SFE, CD, JO; Resources, CD, KNE, RB, MAJ; Data Curation, MWB, SFE, CD, JO; Writing

– Original Draft, MWB, MAJ; Visualisation, MWB, SFE; Supervision, DAN, MAJ; Project Administration, DAN, MAJ; Funding Acquisition, DAN, MAJ.

Acknowledgments

This work was supported by the UKRI (BB/S005404/1, BB/Z514469/1), the Gatsby Charitable Foundation, the Perry Foundation (to SFE), the Douglas Bomford Trust (to SFE) and a William H. Danforth Plant Sciences Fellowship (to KNE).

Declaration of interests

The authors have applied for a patent in relation to this research (PCT/US33/70851).

References

Afgan, E. *et al.* (2016). The Galaxy platform for accessible, reproducible and collaborative biomedical analyses: 2016 update. Nucleic Acids Res **44**:W3-W10.

Arnold, P. A., Kruuk, L. E. B. & Nicotra, A. B. (2019). How to analyse plant phenotypic plasticity in response to a changing climate. New Phytol 222:1235-1241.

Ashburner, M. *et al.* (2000). Gene ontology: tool for the unification of biology. The Gene Ontology Consortium. Nat Genet **25**:25-29.

Balcerowicz, M., Mahjoub, M., Nguyen, D., Lan, H., Stoeckle, D., Conde, S., Jaeger, K. E., Wigge, P. A. & Ezer, D. (2021). An early-morning gene network controlled by phytochromes and cryptochromes regulates photomorphogenesis pathways in Arabidopsis. Mol Plant **14**:983-996.

Bonnot, T., Gillard, M. B. & Nagel, D. H. (2022). CAST-R: An application to visualize circadian and heat stress-responsive genes in plants. Plant Physiology **190**:994-1004.

Bray, N. L., Pimentel, H., Melsted, P. & Pachter, L. (2016). Near-optimal probabilistic RNA-seq quantification. Nat Biotechnol **34**:525-527.

Chen, F., Li, B., Li, G., Charron, J.-B., Dai, M., Shi, X. & Deng, X. W. (2014). Arabidopsis Phytochrome A Directly Targets Numerous Promoters for Individualized Modulation of Genes in a Wide Range of Pathways. The Plant Cell Online **26**:1949-1966.

Chew, Y. H., Seaton, D. D., Mengin, V., Flis, A., Mugford, S. T., George, G. M., Moulin, M., Hume, A., Zeeman, S. C. & Fitzpatrick, T. B. (2022). The Arabidopsis Framework Model version 2 predicts the organism-level effects of circadian clock gene mis-regulation. in silico Plants **4**:diac010.

Clough, S. & Bent, A. (1998). Floral dip: a simplified method for Agrobacterium-mediated transformation of Arabidopsis thaliana. Plant J **16**:735-743.

Covington, M. F., Panda, S., Liu, X. L., Strayer, C. A., Wagner, D. R. & Kay, S. A. (2001). ELF3 modulates resetting of the circadian clock in Arabidopsis. Plant Cell **13**:1305-1315.

Edelstein, A. D., Tsuchida, M. A., Amodaj, N., Pinkard, H., Vale, R. D. & Stuurman, N. (2014). Advanced methods of microscope control using μManager software. J Biol Methods **1**:e10.

Ezer, D. *et al.* (2017). The evening complex coordinates environmental and endogenous signals in Arabidopsis. Nature Plants **3**:17087.

Fehér, B., Kozma-Bognár, L., Kevei, E., Hajdu, A., Binkert, M., Davis, S. J., Schäfer, E., Ulm, R. & Nagy, F. (2011). Functional interaction of the circadian clock and UV RESISTANCE LOCUS 8-controlled UV-B signaling pathways in Arabidopsis thaliana. Plant J **67**:37-48.

Fogelmark, K. & Troein, C. (2014). Rethinking Transcriptional Activation in the Arabidopsis Circadian Clock. PLoS Computational Biology **10**:e1003705.

Franklin, K. A. & Quail, P. H. (2010). Phytochrome functions in Arabidopsis development. J Exp Bot **61**:11-24.

Gene Ontology Consortium. (2023). The Gene Ontology knowledgebase in 2023. Genetics **224**:iyad031.

Graf, A., Schlereth, A., Stitt, M. & Smith, A. M. (2010). Circadian control of carbohydrate availability for growth in Arabidopsis plants at night. PNAS 107:9458-9463.

Guo, W., Tzioutziou, N. A., Stephen, G., Milne, I., Calixto, C. P., Waugh, R., Brown, J. W. S. & Zhang, R. (2021). 3D RNA-seq: a powerful and flexible tool for rapid and accurate differential expression and alternative splicing analysis of RNA-seq data for biologists. RNA Biol **18**:1574-1587.

Hajdu, A., Adam, E., Sheerin, D. J., Dobos, O., Bernula, P., Hiltbrunner, A., Kozma-Bogn√°r, L. & Nagy, F. (2015). High-level expression and phosphorylation of phytochrome B modulates flowering time in Arabidopsis. Plant J **83**:794-805.

Haydon, M. J., Mielczarek, O., Robertson, F. C., Hubbard, K. E. & Webb, A. A. R. (2013). Photosynthetic entrainment of the Arabidopsis thaliana circadian clock. Nature **502**:689-692.

Hicks, K. A., Millar, A. J., Carré, I. A., Somers, D. E., Straume, M., Meeks-Wagner, D. R. & Kay, S. A. (1996). Conditional Circadian Dysfunction of the Arabidopsis early-flowering 3 Mutant. Science (New York, NY) **274**:790-792.

Hsu, P. Y. & Harmer, S. L. (2014). Wheels within wheels: The plant circadian system. Trends in Plant Science **19**:240-249.

Hu, W., Figueroa Balderas, R., Chi Ham, C. & Lagarias, J. C. (2020). Regulation of monocot and dicot plant development with constitutively active alleles of phytochrome B. Plant Direct **4**:401.

Hu, W., Su, Y.-S. & Lagarias, J. C. (2009). A light-independent allele of phytochrome B faithfully recapitulates photomorphogenic transcriptional networks. Mol Plant **2**:166-182.

Huang, D. W., Sherman, B. T. & Lempicki, R. A. (2009). Systematic and integrative analysis of large gene lists using DAVID bioinformatics resources. Nature Protocols **4**:44-57.

Huang, H., Alvarez, S., Bindbeutel, R., Shen, Z., Naldrett, M. J., Evans, B. S., Briggs, S. P., Hicks, L. M., Kay, S. A. & Nusinow, D. A. (2016a). Identification of Evening Complex Associated Proteins in Arabidopsis by Affinity Purification and Mass Spectrometry. Molecular & Cellular Proteomics **15**:201-217.

Huang, H. *et al.* (2017). Cross-species complementation reveals conserved functions for EARLY FLOWERING 3 between monocots and dicots. Plant Direct **1**:e00018.

Huang, H., McLoughlin, K. E., Sorkin, M. L., Burgie, E. S., Bindbeutel, R. K., Vierstra, R. D. & Nusinow, D. A. (2019). PCH1 regulates light, temperature, and circadian signaling as a structural component of phytochrome B-photobodies in Arabidopsis. PNAS **116**:8603-8608.

Huang, H., Yoo, C. Y., Bindbeutel, R., Goldsworthy, J., Tielking, A., Alvarez, S., Naldrett, M. J., Evans, B. S., Chen, M. & Nusinow, D. A. (2016b). PCH1 integrates circadian and light-signaling pathways to control photoperiod-responsive growth in Arabidopsis. eLife **5**

Jiang, Y., Yang, C., Huang, S., Xie, F., Xu, Y., Liu, C. & Li, L. (2019). The ELF3-PIF7 interaction mediates the circadian gating of the shade response in Arabidopsis. iScience **22**:288-298.

Jones, M. A., Hu, W., Litthauer, S., Lagarias, J. C. & Harmer, S. L. (2015). A Constitutively Active Allele of Phytochrome B Maintains Circadian Robustness in the Absence of Light. Plant Physiology **169**:814-825.

Jones, M. A. (2018). Interplay of circadian rhythms and light in the regulation of photosynthesis-derived metabolism. Progress in Botany **79**:147-171.

Jones, M. A. (2019). Retrograde signalling as an informant of circadian timing. New Phytologist **221**:1749-1753.

Jung, J.-H. *et al.* (2016). Phytochromes function as thermosensors in Arabidopsis. Science **354**:886-889.

Jung, J. H. *et al.* (2020). A prion-like domain in ELF3 functions as a thermosensor in Arabidopsis. Nature **585**:256-260.

Kerbler, S. M. & Wigge, P. A. (2023). Temperature Sensing in Plants. Annu Rev Plant Biol **74**:341-366.

Kim, J., Geng, R., Gallenstein, R. A. & Somers, D. E. (2013). The F-box protein ZEITLUPE controls stability and nucleocytoplasmic partitioning of GIGANTEA. Development **140**:4060-4069.

Kolmos, E., Herrero, E., Bujdoso, N., Millar, A. J., T√≥th, R., Gyula, P., Nagy, F. & Davis, S. J. (2011). A reduced-function allele reveals that EARLY FLOWERING3 repressive action on the circadian clock is modulated by phytochrome signals in Arabidopsis. Plant Cell **23**:3230-3246.

Koushik, S. V., Chen, H., Thaler, C., Puhl, H. L. & Vogel, S. S. (2006). Cerulean, Venus, and VenusY67C FRET reference standards. Biophys J **91**:L99-L101.

Laosuntisuk, K., Elorriaga, E. & Doherty, C. J. (2023). The Game of Timing: Circadian Rhythms Intersect with Changing Environments. Annu Rev Plant Biol **74**:511-538.

Legris, M., Klose, C., Burgie, E. S., Rojas, C. C. R., Neme, M., Hiltbrunner, A., Wigge, P. A., Schäfer, E., Vierstra, R. D. & Casal, J. J. (2016). Phytochrome B integrates light and temperature signals in Arabidopsis. Science **354**:897-900.

Liu, X. L., Covington, M. F., Fankhauser, C., Chory, J. & Wagner, D. R. (2001). ELF3 encodes a circadian clock-regulated nuclear protein that functions in an Arabidopsis PHYB signal transduction pathway. Plant Cell **13**:1293-1304.

McWatters, H., Bastow, R., Hall, A. & Millar, A. (2000). The ELF3 zeitnehmer regulates light signalling to the circadian clock. Nature **408**:716-720.

Millar, A. J. (2016). The Intracellular Dynamics of Circadian Clocks Reach for the Light of Ecology and Evolution. Annual Review of Plant Biology **67**:595-618.

Nieto, C., Catalán, P., Luengo, L. M., Legris, M., López-Salmerón, V., Davière, J. M., Casal, J. J., Ares, S. & Prat, S. (2022). COP1 dynamics integrate conflicting seasonal light and thermal cues in the control of Arabidopsis elongation. Sci Adv **8**:eabp8412.

Nusinow, D. A., Helfer, A., Hamilton, E. E., King, J. J., Imaizumi, T., Schultz, T. F., Farr√©, E. M. & Kay, S. A. (2011). The ELF4-ELF3-LUX complex links the circadian clock to diurnal control of hypocotyl growth. Nature **475**:398-402.

Plautz, J. D., Straume, M., Stanewsky, R., Jamison, C. F., Brandes, C., Dowse, H. B., Hall, J. C. & Kay, S. A. (1997). Quantitative analysis of Drosophila period gene transcription in living animals. J Biol Rhythms **12**:204-217.

Pokhilko, A., Fernandez, A. P., Edwards, K. D., Southern, M. M., Halliday, K. J. & Millar, A. J. (2012). The clock gene circuit in Arabidopsis includes a repressilator with additional feedback loops. Mol Syst Biol **8**:574.

Prasetyaningrum, P., Litthauer, S., Vegliani, F., Battle, M. W., Wood, M. W., Liu, X., Dickson, C. & Jones, M. A. (2023). Inhibition of RNA degradation integrates the metabolic signals induced by osmotic stress into the Arabidopsis circadian system. J Exp Bot **74**:5805-5819.

Queiroz, Marina Viana, Battle, M. W. & Jones, M. A. (2023). Interactions between photosynthesis and the circadian system. **Understanding and improving crop photosynthesis: Burleigh Dodds Series in Agricultural Science**:75-92.

R Core Team, R. (2013). R: A language and environment for statistical computing.

Reed, J. W., Nagpal, P., Bastow, R. M., Solomon, K. S., Dowson-Day, M. J., Elumalai, R. P. & Millar, A. J. (2000). Independent action of ELF3 and phyB to control hypocotyl elongation and flowering time. Plant Physiol **122**:1149-1160.

Salome, P. A., To, J. P., Kieber, J. J. & McClung, C. R. (2006). Arabidopsis response regulators ARR3 and ARR4 play cytokinin-independent roles in the control of circadian period. Plant Cell **18**:55-69.

Sanchez, S. E., Rugnone, M. L. & Kay, S. A. (2020). Light Perception: A Matter of Time. Molecular Plant **13**:363-385.

Schneider, C. A., Rasband, W. S. & Eliceiri, K. W. (2012). NIH Image to ImageJ: 25 years of image analysis. Nature Methods **9**:671-675.

Seaton, D. D. *et al.* (2015). Linked circadian outputs control elongation growth and flowering in response to photoperiod and temperature. Molecular Systems Biology **11**:776.

Sherman, B. T., Hao, M., Qiu, J., Jiao, X., Baseler, M. W., Lane, H. C., Imamichi, T. & Chang, W. (2022). DAVID: a web server for functional enrichment analysis and functional annotation of gene lists (2021 update). Nucleic Acids Research **50**:W216-W221.

Somers, D. E., Kim, W. Y. & Geng, R. (2004). The F-box protein ZEITLUPE confers dosage-dependent control on the circadian clock, photomorphogenesis, and flowering time. Plant Cell **16**:769-782.

Somers, D. E., Devlin, P. F. & Kay, S. A. (1998). Phytochromes and cryptochromes in the entrainment of the Arabidopsis circadian clock. Science **282**:1488-1490.

Sorin, C., Salla-Martret, M., Bou-Torrent, J., Roig-Villanova, I. & Martínez-García, J. F. (2009). ATHB4, a regulator of shade avoidance, modulates hormone response in Arabidopsis seedlings. Plant J **59**:266-277.

Su, Y. S. & Lagarias, J. C. (2007). Light-independent phytochrome signaling mediated by dominant GAF domain tyrosine mutants of Arabidopsis phytochromes in transgenic plants. Plant Cell **19**:2124-2139.

Thines, B. & Harmon, F. G. (2010). Ambient temperature response establishes ELF3 as a required component of the core Arabidopsis circadian clock. PNAS **107**:3257-3262.

Ushijima, T. *et al.* (2017). Light Controls Protein Localization through Phytochrome-Mediated Alternative Promoter Selection. Cell **171**:1316-1325.e12.

Wagner, D., Tepperman, J. M. & Quail, P. H. (1991). Overexpression of phytochrome B induces a short hypocotyl phenotype in transgenic Arabidopsis. Plant Cell **3**:1275-1288.

Wang, Q., Liu, W., Leung, C. C., Tarté, D. A. & Gendron, J. M. (2024). Plants distinguish different photoperiods to independently control seasonal flowering and growth. Science **383**:eadg9196.

Webb, A. A. R., Seki, M., Satake, A. & Caldana, C. (2019). Continuous dynamic adjustment of the plant circadian oscillator. Nature communications **10**:550.

Yu, J.-W. *et al.* (2008). COP1 and ELF3 Control Circadian Function and Photoperiodic Flowering by Regulating GI Stability. Molecular Cell **32**:617-630.

Zagotta, M. T., Hicks, K. A., Jacobs, C. I., Young, J. C., Hangarter, R. P. & Meeks-Wagner, D. R. (1996). The Arabidopsis ELF3 gene regulates vegetative photomorphogenesis and the photoperiodic induction of flowering. Plant J **10**:691-702.

Zhang, R. *et al.* (2022). A high-resolution single-molecule sequencing-based Arabidopsis transcriptome using novel methods of Iso-seq analysis. Genome Biol **23**:149.

Zhu, W., Zhou, H., Lin, F., Zhao, X., Jiang, Y., Xu, D. & Deng, X. W. (2020). COLD-REGULATED GENE27 integrates signals from light and the circadian clock to promote hypocotyl growth in Arabidopsis. Plant Cell **32**:3155-3169.

Zielinski, T., Moore, A. M., Troup, E., Halliday, K. J. & Millar, A. J. (2014). Strengths and limitations of period estimation methods for circadian data. PLoS ONE **9**:e96462.

Zuur, A. F., Ieno, E. N., Walker, N. J., Saveliev, A. A. & Smith, G. M. (2009). Mixed effects models and extensions in ecology with R. Springer 574

Figure legends

Figure 1. Modelling suggests COP1-mediated activity is sufficient to integrate phyB signalling into the circadian system. (A) Cartoon of the revised Arabidopsis Framework Model v2 including F2014 circadian model (FMv2+F2014). C2012 and S2015 are distinct modules that model phenology and photoperiodism respectively (Chew et al., 2022). **(B)** PhyB signalling into the circadian system was modelled via two hypotheses. The 'Global phyB effect' variant (upper) proposes that activated phyB is sufficient to induce light-activated gene expression in the circadian system in addition to enabling degradation of COP1. The 'COP1 only' variant (lower) restricts the effect of phyB activation solely to the turnover of COP1. In both cases, stability of ZTL and GI is regulated independently since this is a blue light-mediated effect (Kim et al., 2013). Circadian model adapted from F2014 (Fogelmark and Troein, 2014). Post-translational regulation by light is shown by small white circles. Small red circles indicate post-translational regulation induced by phyB. **(C)** Accumulation of *CCA1*, *LHY*, *GIGANTEA*, and *PRR9* in constant darkness. Plants were entrained in 12:12 light:dark cycles for 12 days before being transferred to constant darkness at dusk (ZT12). Tissue was sampled every 3 hours at the timepoints indicated. Data presented is the average of three independent biological replicates, and is presented relative to accumulation of *APA1, APX3,* and *IPP2* transcripts. Error bars indicate SEM. **(D)** Modelled accumulation of *CCA1m* (*CCA1* mRNA)*, LHYm* (*LHY* mRNA), *GIm* (*GIGANTEA* mRNA), and *PRR9m* (*PRR9* mRNA) in constant darkness. Light grey bars demonstrate subjective day in constant darkness.

Figure 2. *YHBelf3-2* plants lack circadian rhythms but retain modest responses to light cues. (A) Waveforms of luciferase bioluminescence rhythms of wild type (Col-0; black), *YHB* (pink), *elf3-2* (green), and *YHBelf3-2* (purple) seedlings expressing a *CCA1::LUC2* reporter, entrained for 7 days under 12 hr:12 hr light:dark cycles (indicated before timepoint 0 by white and grey bars respectively) before transfer to constant darkness (with subjective day:night cycles in constant darkness indicated by grey and light grey bars after timepoint 0). **(B)** Percentage of seedlings measured in (A) which presented robust circadian rhythms [calculated using BioDare; biodare2.ed.ac.uk; (Zielinski et al., 2014)]. Data are presented as mean ± SEM from three independent experiments. **(C)** Plot showing phase distribution of mis-accumulated transcripts (log2FC > 1.0 or < -1.0 and $p < 0.05$) in each genotype

relative to wild type separated by phase using CAST-R (Bonnot et al. 2022). Y axis depicts fold enrichment compared to reference dataset. Statistical significance was determined using a Chi-square test (Bonnot et al. 2022). Plants were harvested 48 hours after transfer to constant darkness (ZT60). Pyramids indicate up-regulated genes, inverted pyramids represent down-regulated genes; colours as in (A). **(D)** Modelled accumulation of *CCA1m* (*CCA1* mRNA) in 12:12 light:dark cycles. Dark grey bars indicate periods of darkness. **(E)** Patterns of luciferase bioluminescence rhythms of Col-0, *YHB*, *YHBelf3-2* and *elf3-2* seedlings expressing a *CCA1::LUC2* reporter in 12:12 light:dark cycles. **(F)** Phase distribution plot showing time of peak *CCA1*-driven luciferase bioluminescence calculated from (D). Y axis depicts Relative Amplitude Error (RAE). **(G)** Patterns of luciferase bioluminescence rhythms of Col-0, *YHB*, *YHBelf3-2* and *elf3-2* seedlings expressing a *CCA1::LUC2* reporter, entrained for 7 days in pseudo-sinusoidal light conditions (cycles of 1hrs 10 µmol m^{-2} s^{-1}, 8hrs 40 µmol m^{-2} s^{-1}, 6hrs 30 µmol m^{-2} s^{-1}, 3hrs 10 µmol m^{-2} s^{-1} white light followed by 6hrs of darkness). **(H)** Phase distribution plot showing time of peak *CCA1*-driven luciferase bioluminescence calculated from (G). Y axis depicts Relative Amplitude Error (RAE). **(I)** Modelled accumulation of *CCA1m* (*CCA1* mRNA) in constant light. Light grey bars indicate periods of subjective darkness. **(J)** Waveforms of luciferase bioluminescence rhythms of wild type (Col-0), *elf3-2*, *YHB*, and *YHBelf3-2* seedlings expressing a *CCA1::LUC2* reporter, entrained for 7 days under 12 hr:12 hr light:dark cycles and constant 22 °C temperature before transfer to constant light for imaging **(K)** Assessment of rhythmic robustness (Relative Amplitude Error, RAE) plotted against circadian free-running period for data presented in (J). Experimental data are representative of 3 independent experiments (n ≥15). Error bars indicate SEM.

Figure 3. *YHBelf3* plants are less responsive to changing light environments. (A) Modelled hypocotyl length in wild type, *elf3*, *YHB*, and *YHBelf3* seedlings under different simulated photoperiods. **(B)** Representative images of wild type (Col-0), *YHB*, *YHBelf3-2* and *elf3-2* seedlings grown vertically on 0.5 MS plates for five days in constant darkness. **(C)** Quantification of the hypocotyl lengths of Col-0, *YHB*, *YHBelf3-2* and *elf3-2* seedlings grown vertically on 0.5 MS plates for five days in constant darkness. Data shows a representative example from 3 independent experiments (n ≥9). **(D)** Hypocotyl length of Col-0, *elf3-2*, *YHB*

and *YHBelf3-2* seedlings grown vertically on 0.5 MS plates for five days in constant darkness (purple), short day cycles (yellow), long day cycles (orange) or pseudo-sinusoidal light cycles (brown; cycles of 1hrs 10 µmol m^{-2} s^{-1}, 8hrs 40 µmol m^{-2} s^{-1}, 6hrs 30 µmol m^{-2} s^{-1}, 3hrs 10 µmol m^{-2} s^{-1} white light followed by 6hrs of darkness). **(E)** Representative images of Col-0, *YHB*, *YHBelf3-2* and *elf3-2* seedlings grown on soil for 21 days under long day cycles (18 hr:16 hr light:dark) with 150 µmol m^{-2} s^{-1} white light and a constant temperature of 22 °C. **(F)** Rosette diameter of 28 day old Col-0, *elf3-2*, *YHB* and *YHBelf3-2* seedlings grown on soil under short or long days at 22 °C. **(G)** Modelled flowering time in wild type, *elf3*, *YHB*, and *YHBelf3* seedlings under different simulated photoperiods. **(H)** Flowering time of Col-0, *YHB*, *YHBelf3-2* and *elf3-2* plants grown on soil at a constant temperature of 22 °C under long- or short-days. Data shows a representative example from 3 independent experiments (n ≥10). Selected comparisons are presented from a two-way ANOVA analysis, adjusted using Tukey's multiple comparisons test.

Figure 4. *YHBelf3* plants are less responsive to temperature-driven environmental cues. (A) Patterns of luciferase bioluminescence rhythms of wild type (Col-0), *elf3-2*, *YHB*, and *YHBelf3-2* seedlings expressing a *CCA1::LUC2* reporter, entrained for 7 days under 12 hr:12 hr 22 °C:17°C cycles and constant white light before transfer to testing conditions at a constant temperature of 22°C. **(B)** Phase distribution plot showing time of peak *CCA1*-driven luciferase bioluminescence calculated from (A). Data are presented as the mean ± SEM and are representative of at least 3 independent experiments (n ≥ 15). Y axis depicts Relative Amplitude Error (RAE). **(C)** Hypocotyl length of Col-0, *elf3-2*, *YHB* and *YHBelf3-2* seedlings grown vertically on 0.5 MS plates for five days under 12 hr:12 hr light:dark cycles at a constant temperature of (from left to right) 12 °C (blue), 17 °C (light green), 22 °C (dark green), or 27 °C (yellow). **(D)** Rosette diameter of 28 day old Col-0, *elf3-2*, *YHB* and *YHBelf3-2* seedlings grown on soil under 12 hr:12 hr light:dark cycles at a constant temperature of (from left to right) 12 °C (blue), 17 °C (light green), 22 °C (dark green) or 27 °C (yellow). **(E)** Flowering time of Col-0, *elf3-2, YHB*, and *YHBelf3-2* plants grown on soil under 12 hr:12 hr light:dark cycles at a constant temperature of (from left to right) 12 °C (blue), 17 °C (light green), 22 °C (dark green) or 27 °C (yellow). Data are representative of at least three biological repeats.

936 Error bars indicate SEM. Selected comparisons are presented from a two-way ANOVA
937 analysis, adjusted using Tukey's multiple comparisons test. See also Figure S6.
938
939